Journal of Statistical Physics, Vol. 68, Nos. 1/2, 1992

Capture by Stabilized Continuum: Classical and Quantum Aspects

Zi-Min Lu,[1] Michel Vallières,[1] and Jian-Min Yuan[1]

Received December 16, 1991

We review here the results of our investigations concerning chaotic atomic scattering in the presence of a laser field. Particular emphasis is put on the existence of classical stable resonance structures, induced by the intense laser field, which are embedded in the field-free continuum. We show that phase space structures in the vicinity of a resonance island play an important role in the chaotic scattering behavior and form the basis for a mechanism to enhance the lifetimes of the collisional partners. Quantum calculations, based on a wave packet propagation method, show that quantum solutions are strongly influenced by the classical phase space structures. More specifically, a wave packet is found to spread differently in the regular and chaotic regions; in the latter case it spreads exponentially with time until saturation occurs, defining the saturation time. We also investigate the $\hbar$ dependence of the spreading rates in both the regular and chaotic regimes. Calculations with an ensemble of classical trajectories are also presented to further illustrate the smoothing effects of varying $\hbar$.

KEY WORDS: Laser-assisted atomic scattering; stabilized continuum; control of chaos; wave packet propagation; dressed molecular formation; correspondence principle.

1. INTRODUCTION

The classical–quantum correspondence for nonlinear systems is currently a very actively pursued area of research.[1] In particular, great attention has been devoted to the influence of classical phase space structures on quantum dynamics. Stable periodic orbits and surrounding quasiperiodic orbits provide dynamic barriers to quantum flow in addition to the usual static potential barriers, but tunneling through these dynamic barriers has very

[1] Department of Physics and Atmospheric Science, Drexel University, Philadelphia, Pennsylvania 19104-9984.

0022-4715/92/0700-0189$06.50/0

different time characteristics from ordinary potential tunneling (which can be explained by the WKB approximation). This was noted by Davis and Heller in their studies of autonomous systems.[2]

We review in Section 3 a classical control mechanism which we proposed earlier[3,4] to stabilize atom–atom collisional partners under the influence of a laser field and enhance the formation of molecules. This is achieved by switching on the laser field at an appropriate time relative to the collisional process allowing the trapping of the scattering trajectories in the stable structures in the continuum. We will discuss the notion of laser-induced stabilization of the continuum in Section 2.

The concept of dynamical barriers suggests the possibility of realizing the classical control mechanism of scattering events at the quantum level. The feasibility of the dynamical barriers serving to trap incoming wave packets is investigated here by studying the spreading rate and saturation time of arbitrary wave packets originating in regular and chaotic regions of phase space. This will be discussed in Section 4.

The sensitive dependence of the classical scattering function on the initial conditions is somewhat smoothed out in our quantum results. In the last section we carry out a study of the average behavior of an ensemble of classical trajectories over a phase space distribution to provide further understanding of this smoothing effect.

2. CLASSICAL STABILIZED CONTINUUM

We study laser-assisted diatomic collisions in which the two atoms interact via a Morse potential in the presence of a laser field. If we restrict ourselves to head-on collisions with the field also linearly polarized in the same direction, the problem becomes one-dimensional. Using dimensionless variables,[5] we can write the Hamiltonian as

$$H = H_0 + H_{\text{int}} \tag{1}$$

where H_0 is the Hamiltonian describing the interaction of the two atoms using a Morse potential, leading to a dissociation threshold equal to 0.5 in scaled units,

$$H_0 = \frac{p^2}{2} + V_{\text{M}}(x) = \frac{p^2}{2} + \frac{1}{2}(1 - e^{-x})^2 \tag{2}$$

H_{int} is the interaction term between the diatomic system and the laser field in the dipole approximation,

$$H_{\text{int}} = -\mu(x)\, E(\tau) \tag{3}$$

where $\mu(x)$ is the dipole moment of the diatomic system and τ the scaled time. The dipole moment function is assumed to take the form[6]

$$\mu(x) = (x+a)e^{-(x+a)/b} \tag{4}$$

where a and b are related to the zero and the width of μ. We take $a=b=2$ in this paper. The functional form of the dipole moment resembles qualitatively the experimental and calculated results for hydrogen halides.[7]

The laser field $E(\tau)$ is a periodic function of time, and is characterized by a strength A and frequency Ω or the period $T=2\pi/\Omega$. Two kinds of external fields will be considered: a sinusoidal field and a sequence of delta impulses. The former is a more realistic form, while the latter is used to derive analytic results. In the following subsections we will show that the occurrence of stabilization in part of the field-free continuum upon shining an intense laser field onto the two colliding atoms is a generic feature of these systems.

2.1. Sinusoidal Field

In the case of a continuous field we assume that the interaction term takes the form

$$H_{\text{int}} = -A\frac{\Omega}{2}\mu(x)\cos(\Omega\tau) \tag{5}$$

In the numerical experiment we integrate Hamilton's equations for the Hamiltonian defined in (1) and (5) by a Runge-Kutta routine of fourth order. Since the system is driven periodically, we use a stroboscopic representation to study the dynamics. A phase portrait with $A=15$ and $T=0.3$ is shown in Fig. 1. The field-free (ff) ($A=0$) separatrix between the bound and scattering motion, i.e., $H_0=0.5$ curve, is also shown in the same figure by a dotted line. We observed that the phase portrait is dominated by a saddle point and its stable and unstable manifolds in the part of phase space for which the bound motion under the exposure of the laser field now lies outside the ff separatrix.

To understand the observed features in phase space, we derive an effective potential in the high-frequency limit by separating the dynamics into rapidly and slowly varying parts[8]; this allows us to average the effect of the rapidly varying part of the motion and produces the time average effective potential guiding the slow particle motion. For our system, this leads to the following effective potential:

$$V_{\text{eff}}(x) = V_{\text{M}}(x) + \frac{A^2}{16}\left(\frac{d\mu}{dx}\right)^2 \tag{6}$$

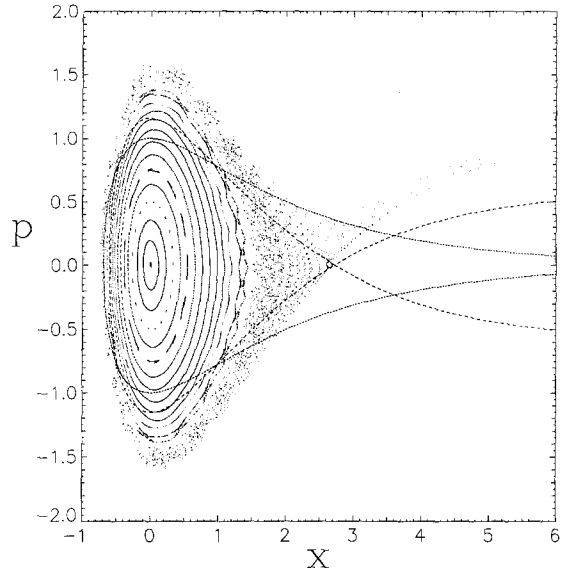

Fig. 1. Stroboscopic section for sinusoidally driven atomic collision with field parameters $A = 15$ and $T = 0.3$. The period-1 saddle point is located at $(x, p) = (2.647856, 0)$ and is indicated by a small circle. The dashed line denotes the homoclinic orbit or the effective potential. The dotted line shows the field-free (ff) separatrix.

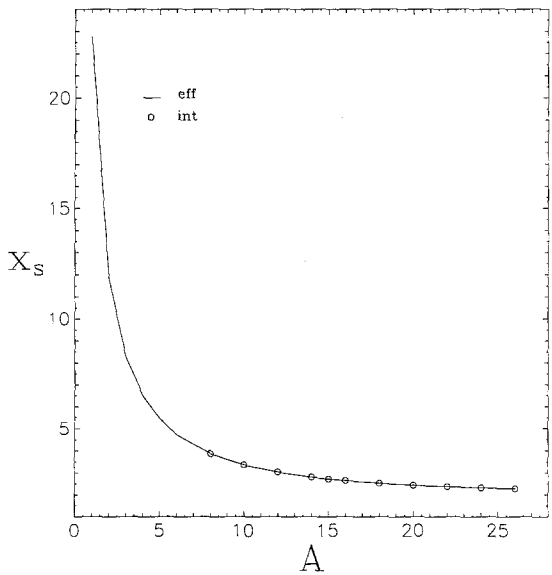

Fig. 2. The saddle location x_s as function of the field strength A according to the effective potential theory. The circles represent the period-1 saddle points as found by numerical search.

where V_M is the Morse potential. The coordinate of a maximum for the effective potential x_s is given by the nonzero root of the following equation:

$$\frac{dV_M}{dx} + \frac{A^2}{8}\frac{d\mu}{dx}\frac{d^2\mu}{dx^2} = 0 \tag{7}$$

This maximum corresponds to a saddle point at $(x_s, p_s = 0)$. In Fig. 2 we plot x_s as a function of the field strength A.

We observe in Fig. 2 that the saddle point moves inward along the x axis and approaches 2 as A increases since $(d\mu/dx)^2$ peaks at $x = a = 2$. The separatrix between bound and unbound motion under the influence of the effective potential is the homoclinic orbit given by the equation

$$H_{\text{eff}}(x) = \frac{p^2}{2} + V_{\text{eff}}(x) = V_{\text{eff}}(x_s) \tag{8}$$

In Fig. 3 the homoclinic orbits of the effective potential are plotted for various A. As A increases, the enclosed phase space region is squeezed along the x axis and elongated along the p axis, leading to a portion of the enclosed region being outside the ff separatrix. This opens up the possibility that a part of the stable KAM zone extends into the continuum. Without the field the continuum is flatly unstable, but with the field on part of the continuum may become stable; this region becomes accessible through a

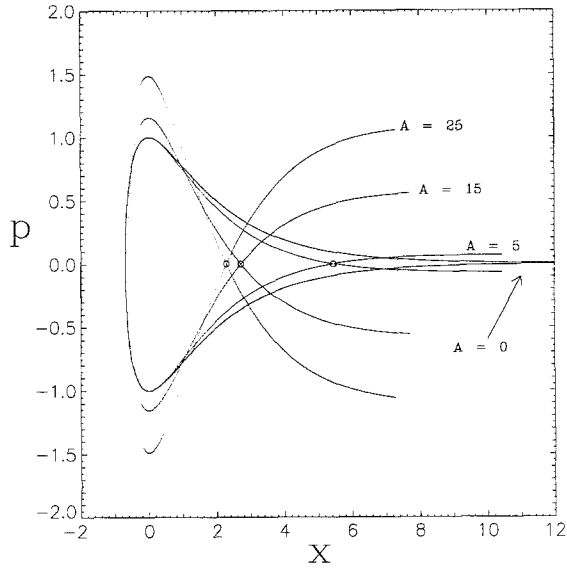

Fig. 3. The homoclinic orbits of the effective potential theory for different field strengths.

scattering process when the field is gradually switched on. We call the stable region outside the ff separatrix the *stabilized continuum.*

We use an algorithm[9] based on linearization around a trial orbit to find the saddle periodic orbits associated with the homoclinic orbits. In Fig. 2 the circles represent the results from the search. Since $\Omega = 2\pi/T \approx 21 \gg \omega_{\text{Morse}} \approx 1$ is used, we indeed have good agreements between the effective potential theory and the numerical integration.

The bulk features in Fig. 1 are well explained by the effective potential; for instance, the stable zone extending outside the ff separatrix is due to a deeper effective potential well than the ff well. Of course the driven system whose stable and unstable manifolds intersect transversely at homoclinic points is nonintegrable. These homoclinic tangles are responsible for the emerging chaotic behavior, since they imply the existence of a countably infinite number of periodic orbits.

2.2. Impulsive Field

Here we replace the driving term by a series of δ-functions (Dirac comb) by requiring the average of the driving term over a half period to be the same as that of the series of δ-functions over one period, leading to

$$H_{\text{int}} = -A\mu(x) \sum_{n=-\infty}^{n=+\infty} \delta(\tau - nT) \tag{9}$$

where $T = 2\pi/\Omega$ is the period of the driving field.

Integrating Hamilton's equations of motion, we get an area-preserving map M which is piecewise analytical depending on whether the energy $E = H_0$ of the Morse oscillator is below or above the dissociation threshold.[4] If we synchronize the map on the time just prior to the impulse, the map M is naturally decomposed into an impulse K followed by a free evolution F under the Morse potential for one period T of the external field, namely

$$\begin{pmatrix} x_{n+1} \\ p_{n+1} \end{pmatrix} = M \begin{pmatrix} x_n \\ p_n \end{pmatrix}, \qquad M = F \circ K \tag{10}$$

The impulsive term K is obtained by solving Hamilton's equations from just before an impulse to just after; it changes the momentum impulsively and keeps x fixed. The free-evolution term F propagates the trajectory for a period T ahead along the constant-energy E curve,

$$\begin{pmatrix} E \\ \theta + \omega T \end{pmatrix} = F \begin{pmatrix} E \\ \theta \end{pmatrix} \tag{11}$$

where $\omega = \omega(E)$ is the frequency of the Morse oscillator.

The stabilized continuum in this case comes from a period-one saddle–center bifurcation.[10] As A increases, a period-three saddle–center bifurcation occurs. Then the period-three center undergoes a period-doubling cascade while the period-three saddle moves toward the stable period-one center, leading to a stable resonance island with a triangular shape. Upon further increasing A the period-one center orbit can collide with the period-three saddle orbit to form a periodic orbit associated with a 3:1 resonance.[11] The period-one center and the period-three saddle then reemerge after the collision, leading again to a triangular stable island but with reversed orientation. The resonance island is outside the ff separatrix, therefore lying in the continuum, as shown in Fig. 4 for $A = 2e^2$ and $T = 5.271719$.

An expansion for the forcing function $d\mu/dx$ up to quadratic terms at $x = a$ leads to a valid local approximation to K since $d\mu/dx$ peaks at $x = a$. Further, if we replace F by a rotation R, which is equivalent to replacing the Morse potential by a harmonic oscillator potential, the map (10) is locally reduced to a Hénon map.[4] Linking numbers[10] for periodic orbits

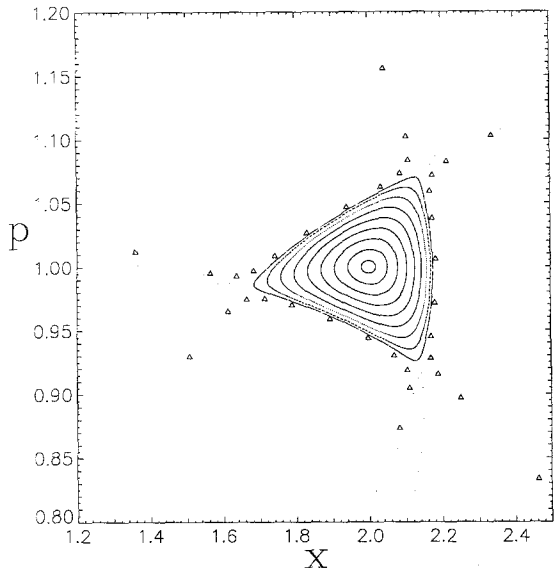

Fig. 4. Stroboscopic map (in which x and p are recorded prior to each impulse) showing the KAM curves, which form a resonant island in the vicinity of the period-one orbit located at $(x, p) = (2, 1)$ with energy 0.873823 when the field parameters are $A = 14.77811$ and $T = 5.271719$. The "dots" are computed by a multiple iterations of the map for an ensemble of initial conditions near the period-one orbit. The "triangles" are the stroboscopic map of a particular scattering trajectory.

can be calculated, which provides "selection rules" for periodic orbits to interact (creation or annihilation) and confirms the observed bifurcation sequence.

3. CONTROLLING CHAOTIC SCATTERING

Chaotic scattering in the presence of an intense laser field can be understood in terms of the stable manifolds of the unstable periodic orbits, extended into the asymptotic region. The intersection of these manifolds with the initial condition line is fractal, thus nondifferentiable with respect to the initial conditions, so that small differences in the initial conditions can lead to totally different scattering results.

A part of the ff continuum becomes stable because of the presence of the intense field. Then an immediate application of our finding follows: field-dressed molecules can be formed by switching on the field when the trajectories get into the stable islands. This is possible since those stable islands lie in the field-free continuum and are thus accessible via a scattering process before the field is fully turned on.

In this sense the chaotic scattering can be controlled by bringing the trajectories into the stable resonance region. Two examples[3, 4] are shown in Fig. 5, one for the continuous field and another for the impulsive field.

4. QUANTUM DYNAMICS

To study the quantum dynamics of this problem, we use a direct approach in solving the Schrödinger equation numerically, We use a standard implicit numerical method,[12] summarized by the following formula:

$$\Psi^{n+1} = \frac{1 - i\frac{1}{2} H\,\delta t}{1 + i\frac{1}{2} H\,\delta t}\,\Psi^{n} \tag{12}$$

expressing the time evolution over a small time step. This method maintains unitarity; we use a three-point formula for the second differential operator for efficiency. We have also compared the solution obtained by this approach to the solution obtained by the Feit–Fleck spectral method[13] and found good agreement. For both methods we have introduced an absorbing boundary[14] at a large positive x to avoid the reflection from the grid boundary.

To emulate the launching of classical particles from position x and

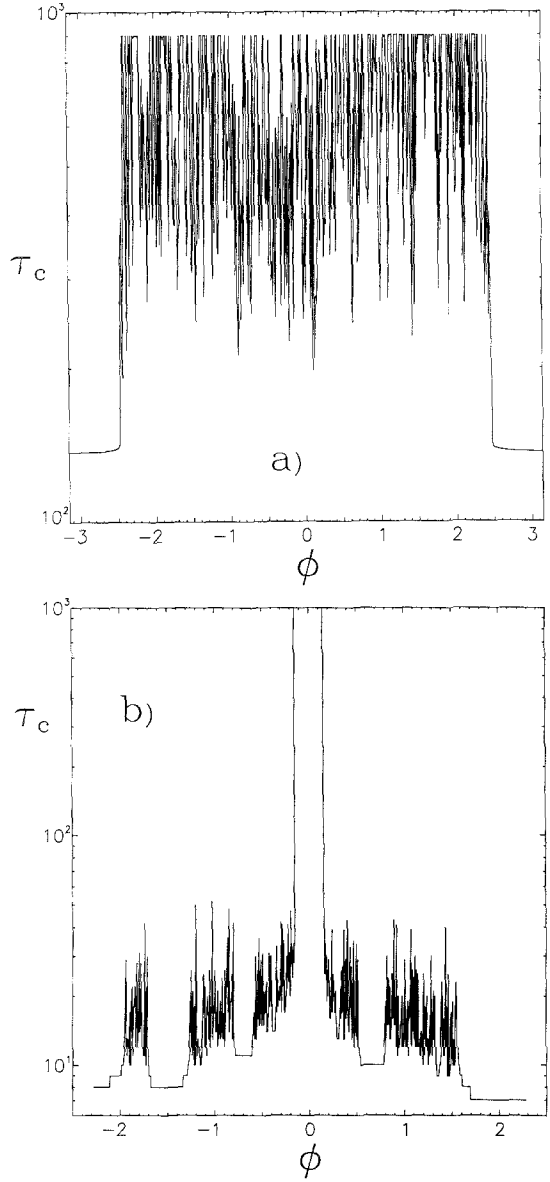

Fig. 5. (a) The scattering times for an ensemble of 500 scattering trajectories that initiate at $(x, p) = (19.994151, -9.627211 \times 10^{-2})$ with uniformly distributed phases in the interval $-\pi, +\pi$ for field parameters $A = 15$ and $T = 0.3$ and switching function of width $t_s = 10T$. (b) The scattering times of an ensemble of trajectories of a given initial momentum $p_0 = -0.864665$ and initial x located in a small interval centered at $x_0 = 20.389025$ of width $|p_0| T = 4.558271$ to simulate different relative phases $[-\pi, +\pi]$ between the Morse oscillator and the impulsive field, when the field is suddenly turned on.

momentum p, we start a Gaussian wave packet with minimal uncertainty commensurate with the size of $\hbar$ (a Glauber coherent state),

$$\psi(x, t=0) = C \exp\left(\frac{i}{\hbar} p_0 x - \frac{(x-x_0)^2}{4\sigma_x^2}\right) \tag{13}$$

where $C = (2\pi\sigma_x^2)^{-1/4}$, and observe its time evolution. Note that in our dimensionless units $\hbar$ is inversely proportional to the number of bound states that the Morse potential can support.

4.1. Time Scales for Spreading of Wave Packets

The rate of spreading of a localized wave packet in different parts of classical phase space can be quite different[15]; this is due to the fact that the phase space is mixed with regular and chaotic regions. On the other hand, the control mechanism suggested in Section 3 depends on the stable structures in the phase space. Those stable islands correspond locally to an integrable system, despite the overall nonintegrability, and therefore will lead to a wave packet spreading rate typical of integrable systems. It is believed that the spreading rate in a regular region is much slower than in a chaotic region. To confirm this idea, we use the product $\sigma_x \sigma_p$ of the mean deviations of x and p to investigate the spreading of the wave packet starting inside the near-integrable stable islands. Classically, due to the

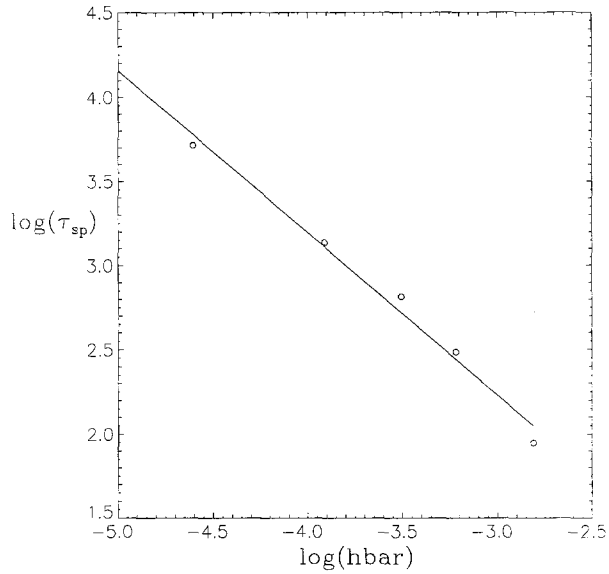

Fig. 6. The spreading time t_{sp} as function of $\hbar$ where the field parameters are the same as in Fig. 4.

area-preserving property of Hamiltonian dynamics, the product should remain constant for a short duration. Thus the effect of the quantum diffusion can be characterized by the time dependence of the product.

Starting with a wave packet with minimal uncertainties in x and p, (13), we define the spreading time τ_{sp} as the first time when the smoothed product $\sigma_x \sigma_p$ exceeds the area of the triangular region (Fig. 4). In Fig. 6 we present a log–log plot for the spreading time τ_{sp} as function of $\hbar$. A linear fit to the curve suggests

$$\tau_{sp} \sim \frac{1}{\hbar} \tag{14}$$

in this regular region.

For regions where the classical dynamics is chaotic, we need a quantity which can reflect the stretching and folding properties of the classical phase flow. The product $\sigma_x \sigma_p$ fails to give any useful clues in this respect since it is classically a constant for a short time interval. Instead we focus on the spreading σ_u along the direction of the classical unstable manifold for such a signal; this quantity leads to the quantum equivalent of the Lyapunov exponent.

We start the wave packet at the location of a period-one flip-saddle point where the linearized map has eigenvalues $\lambda_1 = 1/\lambda_2 = -2.069019$ for $A = 2e^2$ and $T = 6.8$. The flip-saddle results from a period-doubling bifurcation of the stable period-one center as T increases from 6.05 with the same A. Plotting $\log(\sigma_u)$ as a function of time for several $\hbar$ ranging from 0.01 to 0.03, we find in general a linear growth followed by saturation. Typical examples are shown in Fig. 7. We call the time at which saturation first occurs the saturation time τ_s. In Table I we list the results for the saturation time and slope α_q of the linear rising part. The slope is the quantum analog to the classical *Lyapunov exponent*, which in this case equals $(1/T)\log(|\lambda_1|) = 0.106922$. It is interesting to note that $\alpha_q \tau_s \sim 1$, that is, the saturation time is $\sim 1/\alpha_q$.

Table I. $\hbar$ Dependence of the Saturation Time and α_q

$\hbar$	τ_s	α_q
0.010	22	0.03520
0.012	20	0.06137
0.014	18	0.07271
0.016	16	0.07798
0.018	15	0.08465
0.020	12	0.09241
0.030	9	0.10510

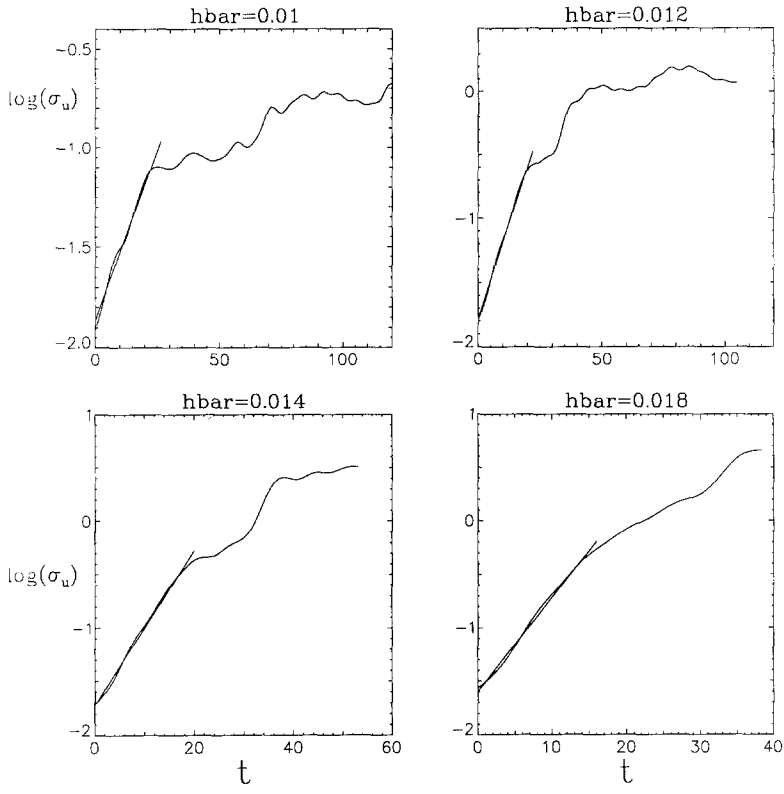

Fig. 7. The spread along the direction of the unstable manifold σ_u as a function of time for $A = 2e^2$, $T = 6.8$, and $\hbar = 0.01$, 0.012, 0.014, and 0.018, respectively.

Heller[16] defined a *break time* as the time to resolve features differing in energy by ΔE which is inversely proportional to the local density of states for bound regions. The saturation time introduced above might also be considered as a *break time.*

4.2. Enhancement of Scattering Times

In this section we discuss the increase of quantum scattering time due to the stabilized continuum in the classical phase space. We use first the impulsive field case as an example to illustrate the mechanism and discuss the continuous field case latter in this section.

The first question we address is concerned with the existence of "*trapping*" in the quantum mechanical solution. Namely, we conjecture

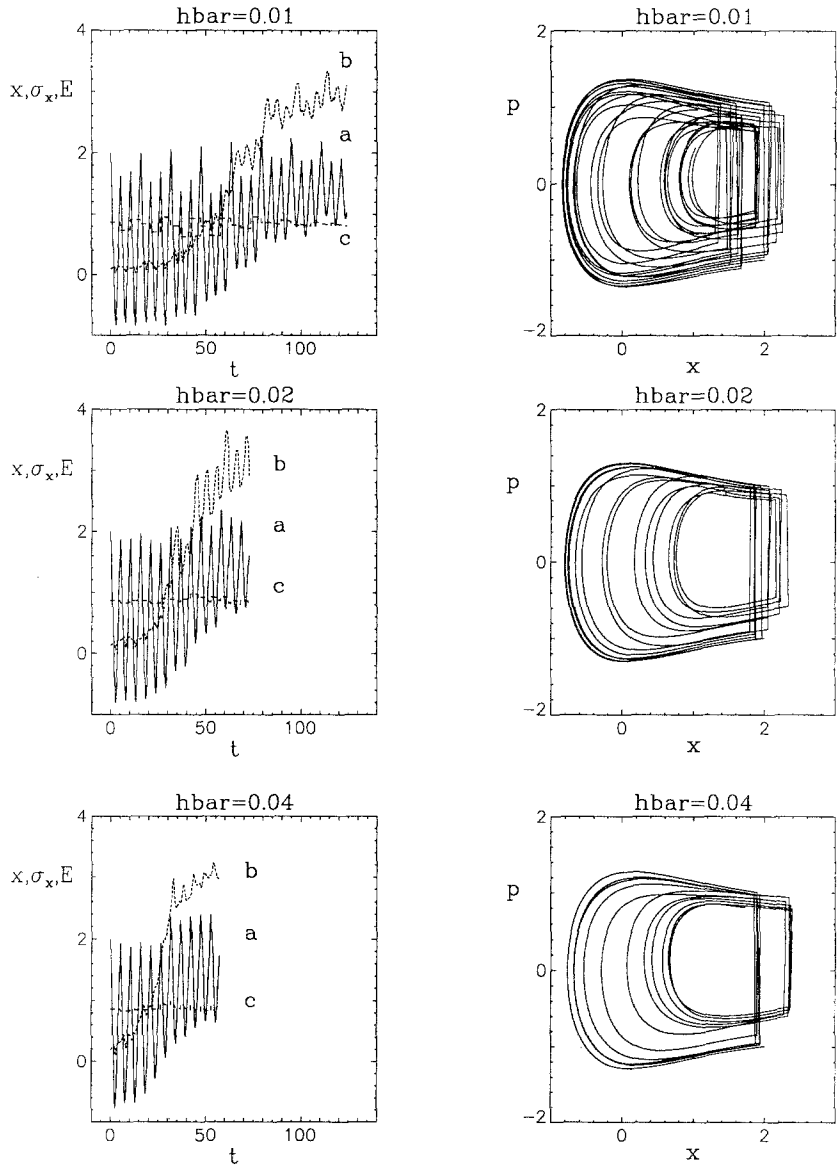

Fig. 8. Quantum time evolution of a wave packet originally centered within the classical triangular structure. The RHS figures show a "*phase space portrait*" in terms of expected values. The LHS figures show (a) $\langle x \rangle$, (b) spread in x, and (c) energy of the solution for various $\hbar$.

that the triangular structure surrounding the period-one orbit will influence the quantum solution provided it has an area large enough compared to $\hbar$.

To illustrate this point, we launched a Gaussian wave packet within the triangular structure. Figure 8 shows the results of such calculations. The "*quantum trajectories*" were obtained by plotting the momentum expected value $\langle p \rangle$ versus the position expected value $\langle x \rangle$. We recognize that the equivalence of the period-one orbit is well reproduced, but that eventually the wave packet will spread out, presumably due to dynamical tunneling.[2] Quantum mechanics allows for a spreading of the wave packet; the left panel of Fig. 8 shows that the widening of the wave packet is prevalent and that the diffusion rate is larger for larger $\hbar$. Thus, these results are consistent with the conjecture that quantum results approach the classical results as $\hbar$ decreases.

As stated earlier, the spreading is much faster in the classical chaotic region than in the regular region, since both quantum dispersion and classical stochasticity are present in the chaotic region. This difference in quantum time scale will enhance the possibility of our control mechanism. Before turning on the laser field, the classical phase space is regular; after

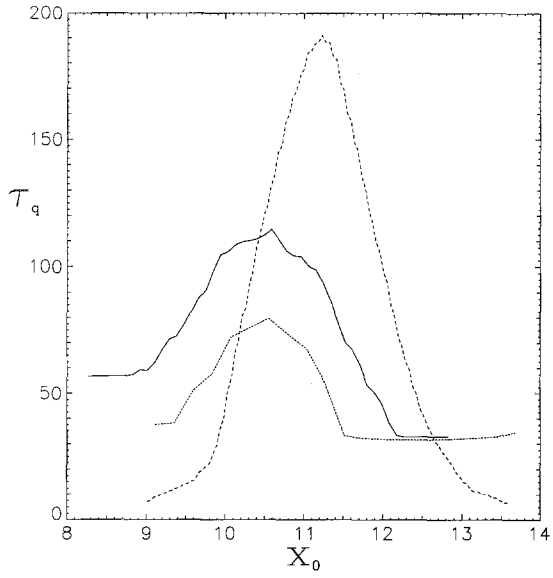

Fig. 9. The lifetime as function of the initial position of the wave packet with $p_0 = -0.864665$ and $\hbar = 0.01$. The field is turned on after four optical cycles with the field parameters the same as in Fig. 4. The solid line is for the exit probability $P_{\text{exit}} = 0.6$ and the dotted line is for $P_{\text{exit}} = 0.8$. The dashed line shows the average results of an ensemble of classical trajectories distributed according to the initial quantum wave packet probability profile.

switching on the laser field, the system is locally integrable in the resonance region, which leads to a spreading rate typical of integrable systems. A wave packet with the right initial conditions which is caught by the resonance structure will have a spreading, mainly due to dynamical tunneling out of the resonance island, much slower than the spreading of a similar wave packet with slightly different initial conditions which might end up in the classical chaotic region after the field is turned on. This indicates that the control mechanism we proposed earlier ought to work for the quantum system as well.

In Fig. 9 we show the lifetime as function of the initial position of the wave packet. The field is switched on after four optical cycles. The norm of the wave packet is used as a criterion to define the lifetime, the time for the norm to reach P_{exit}. Two sets of results with $P_{\text{exit}} = 0.8$ and 0.6 are shown in Fig. 9. The lifetime enhancement is apparent; the wave packets with the

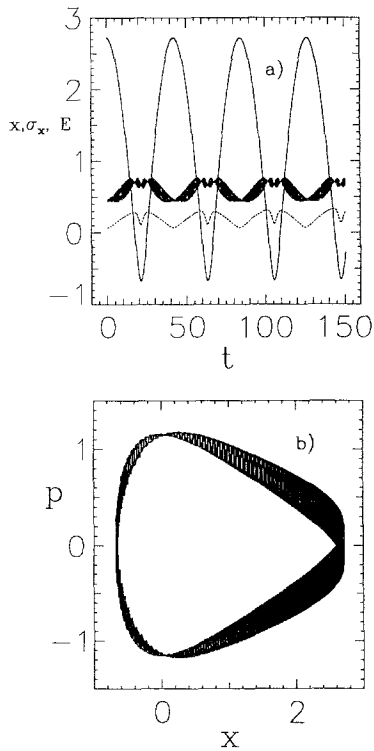

Fig. 10. Quantum time evolution of a wave packet originally centered at the saddle point $(x_s, p_s) = (2.647856, 0)$ and $\hbar = 0.01$. (a) $\langle x \rangle$ (solid line), the spread in x (dotted line), and the energy for three orbital periods (about 300 optical periods). The field parameters are the same as in Fig. 1. (b) A "*phase space portrait*" in terms of expected values.

right initial conditions to be caught by the stable structures have longer lifetimes.

We have found that the enhancement of scattering time is also remarkable for the continuous driven case. In Fig. 10 we show a calculation of wave packet evolution starting at the classical saddle point associated with the homoclinic orbits. The mean values of the position and momentum follow the classical homoclinic orbits of the effective potential over many (>500) optical periods. We also plot $\langle x \rangle$, σ_x, and E in Fig. 10 as functions of time. We clearly see that the spreading is very slow.

5. AVERAGING OF CLASSICAL OBSERVABLES OVER PHASE SPACE DISTRIBUTION

The initial Gaussian wave packet has minimal uncertainties over x and p given by $\sigma_x = \sigma_p = (\hbar/2)^{1/2}$. To simulate the corresponding probability distribution, we launch an ensemble of classical trajectories distributed over phase space according to the Husimi density distribution,

$$\mathscr{P}_{x_0, p_0}(x, p; \hbar) = \exp\left(-\frac{(x-x_0)^2}{4\sigma_x^2} - \frac{(p-p_0)^2 \sigma_x^2}{\hbar^2} \right) \tag{15}$$

of the initial wave packet (13). The averaged observables $\Gamma(x_0, p_0; \hbar)$ can be calculated from the classical quantity $\Gamma_c(x, p)$ according to

$$\Gamma(x_0, p_0; \hbar) = \int dx \int dp \, \mathscr{P}_{x_0, p_0}(x, p; \hbar) \, \Gamma_c(x, p) \tag{16}$$

The width of the Husimi distribution is a function of $\hbar$; in the classical ensemble calculations which follow we will use $\hbar$ as a free parameter to monitor the width of the averaging process.

The averaged scattering time is shown in Fig. 9 for $\hbar = 0.01$ as a function of x_0 with $p_0 = -0.864665$. The sensitivity of the collision times over the initial conditions is smoothed out by the averaging process and the resulting width of the lifetime distribution is comparable to that of the quantum calculation, also shown in Fig. 9. The peak position of the classical calculation is shifted to a higher x_0 value than the corresponding quantum one and the asymmetric shape of the quantum distributions does not show in the classical result. These subtle effects need further understanding. The sensitive dependence of the scattering time reemerges at lower values of $\hbar$, the width monitoring parameter of the classical ensemble distribution. In the limit of small $\hbar$, $\mathscr{P}_{x_0, p_0}(x, p; \hbar)$ behaves like $\delta(x-x_0)\,\delta(p-p_0)$, so that the average lifetime reduce to τ_c.

6. CONCLUSIONS

We have discussed in this paper the classical and quantum behavior of laser-assisted atom–atom collisions. In the classical approach we have observed a mix of regular and chaotic behavior in phase space. Most interestingly, we have illustrated that stable structures appear in the field-free continuum of the Morse potential under the influence of the laser field. These structures could be used to enhance molecular formation by switching on the laser field at an appropriate time relative to the collision process. We have reported on quantum results which support our classical control mechanism. An interesting question concerns the spreading rates of wave packets in the regular and chaotic regions. We have studied the spread in phase space of Gaussian wave packets of minimum uncertainty and found a power law dependence, $1/\hbar$, for wave packets originating in the classically regular region. In the chaotic regime, on the other hand, results reveal an exponential spread in the classical unstable direction followed by saturation; the $\hbar$ dependence of the characteristic time in the exponential growth and the saturation times have been calculated.

The quantum results show that the fine structures in the classical chaotic scattering region are somewhat smoothed out for larger $\hbar$. We have illustrated this effect via an ensemble calculation over classical trajectories using a probability profile based on the phase space distribution corresponding to a minimum-uncertainty Gaussian wave packet. The width of this phase space distribution is characterized by the parameter $\hbar$. Even though the sensitive dependence over initial conditions is somewhat smoothed out for large $\hbar$, it remains very evident for small values of $\hbar$.

A recent attempt at understanding the phenomena of trapping and quantum localization leads to the concept of a vortex tube[17] in classical phase space; it was found that quasienergy states were strongly influenced by these structures. This concept might provide a fundamental understanding of the trapping and control mechanism we have discussed in the context of molecular scattering. We are currently investigating this connection.

ACKNOWLEDGMENTS

This work was supported partially by the NSF through Grant No. Phy 90-04582 and the donors of the Petroleum Funds, administered by the ACS. We acknowledge Cray supercomputer time from NCSA.

REFERENCES

1. M. C. Gutzwiller, *Chaos in Classical and Quantum Mechanics* (Springer-Verlag, New York, 1990); B. Eckhardt, *Phys. Rep.* **163**:205 (1988); M. V. Berry and E. J. Heller,

in *Lectures of the Les Houches School on Chaos and Quantum Physics* (North-Holland, Amsterdam, 1990); J. F. Heagy, Z. M. Lu, J. M. Yuan, and M. Vallières, Dynamics of driven molecular systems influenced by phase space structures, in *Directions in Chaos*, Vol. IV, D. H. Feng and J. M. Yuan, eds., to appear.
2. M. J. Davis and E. J. Heller, *J. Chem. Phys.* **75**:246 (1981); E. J. Heller, *Chem. Phys. Lett.* **60**:328 (1979).
3. Zi-Min Lu, Michel Vallières, and Jian-Min Yuan, Controlling chaotic scattering: Stimulated molecular recombination, *Phys. Rev. Lett.*, submitted.
4. Zi-Min Lu, Michel Vallières, Jian-Min Yuan, and Jim Heagy, Controlling chaotic scattering: I—Impulsively driven Morse oscillator, *Phys. Rev. A*, in press.
5. J. F. Heagy and J. M. Yuan, *Phys. Rev. A* **41**:571 (1990); J. Heagy, Ph.D. thesis, Drexel University (1990), unpublished.
6. Gerhard Herzberg, *Molecular Spectra and Molecular Structure I. Spectra of Diatomic Molecules* (Van Nostrand, Toronto, 1950); R. Heather and H. Metiu, *J. Chem. Phys.* **86**:5496 (1987).
7. J. F. Ogilvie, W. R. Rodwell, and R. H. Tipping, *J. Chem. Phys.* **73**:5221 (1980).
8. L. D. Landau and E. M. Lifshitz, *Mechanics*, 3rd ed. (Pergamon Press, 1976).
9. Ira Bruce Schwartz, *SIAM J.* **20**:106 (1983).
10. Zi-Min Lu *et al.*, Bifurcation and linking number of periodic orbits in an area-preserving map, Preprint, Drexel University (1991).
11. V. I. Arnold, *Mathematical Methods of Classical Mechanics* (Springer-Verlag, New York, 1978); D. K. Arrowsmith and C. M. Place, *An Introduction to Dynamical Systems* (Cambridge University Press, Cambridge, 1990).
12. S. E. Koonin and D. C. Meredith, *Computational Physics* (Addison-Wesley, 1990).
13. M. D. Feit, J. A. Fleck, Jr., and A. Steiger, *J. Comput. Phys.* **47**:412 (1982).
14. R. Heather and H. Metiu, *J. Chem. Phys.* **86**: 5009 (1987); **88**:5496 (1988); R. B. Gerber, R. Kosloff, and M. Berman, *Comput. Phys. Rep.* **5**:59 (1986).
15. G. P. Berman, V. Yu. Rubaev, and G. M. Zaslavsky, *Nonlinearity* **3**:1 (1991).
16. E. J. Heller, in *Quantum Chaos and Statistical Physics*, T. H. Seligman and H. Nishioka, eds. (Springer-Verlag, Berlin, 1986).
17. H. P. Breuer and M. Holthaus, *Ann. Phys.* (N.Y.) **211**:249 (1991).